ELSEVIER

International Journal of Heat and Fluid Flow 21 (2000) 599–605

International Journal of HEAT AND FLUID FLOW

www.elsevier.com/locate/ijhff

Structure-based turbulence modeling for wall-bounded flows

Stavros C. Kassinos *, Carlos A. Langer, Scot L. Haire, William C. Reynolds

Department of Mechanical Engineering, Stanford University, Stanford, CA 94305, USA

Abstract

The performance of Reynolds stress transport (RST) models in non-equilibrium flows is limited by the lack of information about two dynamically important effects: the role of energy-containing turbulence structure (dimensionality) and the breaking of reflectional symmetry due to strong mean or frame rotation. Both effects are fundamentally non-local in nature and this explains why it has been difficult to include them in *one-point* closures like RST models. Information about the energy-containing structure is necessary if turbulence models are to reflect differences in dynamic behavior associated with structures of different dimensionality (nearly isotropic turbulence vs turbulence with strongly organized two-dimensional structures). Information about the breaking of reflectional symmetry is important whenever mean rotation is dynamically important (flow through axisymmetric diffuser or nozzle with swirl, flow through turbomachinery, etc.). Here we present a new one-point model that incorporates the needed structure information, and show a selection of results for homogeneous and inhomogeneous flows.

1. Introduction

Reynolds-averaged turbulence models are the primary tools for the engineering analysis of complex turbulent flows, but their performance in flows that must be computed in order to advance technology is at best inconsistent. Dynamically important features of the turbulence structure are inherently non-local in nature, and thus difficult to emulate in one-point closures, yet they cannot be completely ignored in models that are designed for use in complex flows. This lack of crucial information is now recognized as one of the primary challenges facing one-point turbulence modeling.

Consider for example the case of Reynolds stress transport (RST) models, where the Reynolds stresses R_{ij} are used for closing the unknown terms in their own transport equations. R_{ij} carries information about the *componentality* of the turbulence (the relative strengths of different velocity components), but not about its *dimensionality* (the relative uniformity of the structure in different directions). Thus RST models cannot possibly satisfy conditions associated with the dimensionality of the turbulence, or reflect differences in dynamic behavior associated with structures of different dimensionality (nearly isotropic turbulence vs turbulence with strongly organized two-dimensional structures). Similarly, well-known limitations of RST models in predicting flows with strong rotation can be, at least partly, traced back to the lack of dimensionality and other information.

In the issues outlined above, and discussed in more detail in Reynolds and Kassinos (1995) and Kassinos et al. (1999), let us, introduce a set of one-point turbulence structure tensors that contain key information missing from standard one-point closures. Here, we outline the construction of a one-point model based on the transport of one of these tensors, and show a selection of results for homogeneous and inhomogeneous flows.

2. Definitions

We introduce the turbulent stream function Ψ'_i, defined by

$$u'_i = \epsilon_{itz}\Psi'_{z,t}, \quad \Psi'_{i,i} = 0, \quad \Psi'_{i,nn} = -\omega'_i, \tag{1}$$

where u'_i and ω'_i are the fluctuating velocity and vorticity components. The Reynolds stress tensor is given by

$$R_{ij} = \overline{u'_i u'_j} = \epsilon_{ipq}\epsilon_{jts}\overline{\Psi'_{q,p}\Psi'_{s,t}}, \tag{2a}$$

and the associated non-dimensional and anisotropy tensors are

$$r_{ij} = R_{ij}/q^2, \quad \tilde{r}_{ij} = r_{ij} - \frac{1}{3}\delta_{ij}. \tag{2b}$$

Here $q^2 = 2k = R_{ii}$. Using isotropic tensor identities (Mahoney, 1985), we can write (2a) as

$$R_{ij} + \underbrace{\overline{\Psi'_{k,i}\Psi'_{k,j}}}_{D_{ij}} + \underbrace{\overline{\Psi'_{i,k}\Psi'_{j,k}}}_{F_{ij}} - \underbrace{\left(\overline{\Psi'_{i,k}\Psi'_{k,j}} + \overline{\Psi'_{j,k}\Psi'_{k,i}}\right)}_{C_{ij}+C_{ji}} = \delta_{ij}q^2. \tag{3}$$

The constitutive equation (3) shows that one-point correlations of stream-function gradients, like the Reynolds stresses, are dominated by the energy-containing scales. These correlations contain independent information that is important for the proper characterization of non-equilibrium turbulence. For example, the D_{ij} tensor reveals the level of two-dimensionality

* Corresponding author. Tel.: +1-650-723-0546; fax: +1-650-723-4548.

E-mail address: kassinos@eddy.stanford.edu (S.C. Kassinos).

0142-727X/00/$ - see front matter
PII: S0142-727X(00)00050-3

(2D) of the turbulence, and F_{ij} describes the large-scale structure of the vorticity field (Reynolds and Kassinos, 1995).

In homogeneous turbulence, the new structure tensors are most conveniently defined in terms of their associated spectra. It is useful to recall that in this case, discrete Fourier expansions can be used to represent individual realizations in a box of length L. Then the discrete cospectrum of two fields **f** and **g** is given by

$$\tilde{X}_{ij}(\mathbf{k}) = (L/2\pi)^3 \overline{\hat{f}_i(\mathbf{k})\hat{g}_j^*(\mathbf{k})},$$

where the bar represents an ensemble average over the box. The cospectrum of two fields $X_{ij}(\mathbf{k})$ is the limit of the discrete cospectrum $\tilde{X}_{ij}$ as $L \to \infty$. Here we use

$$X_{ij}(\mathbf{k}) \sim \overline{\hat{f}_i(\mathbf{k})\hat{g}_j^*(\mathbf{k})}$$

as a shorthand notation, but the exact definition should be kept in mind.

For homogeneous turbulence $C_{ij} = C_{ji} = 0$, and the remaining tensors in (3) have equivalent representations in terms of the velocity spectrum tensor $E_{ij}(\mathbf{k}) \sim \overline{\hat{u}_i\hat{u}_j^*}$ and the vorticity spectrum tensor $W_{ij}(\mathbf{k}) \sim \overline{\hat{\omega}_i\hat{\omega}_j^*}$. These are given below.

Structure *dimensionality* tensor:

$$D_{ij} = \int \frac{k_i k_j}{k^2} E_{nn}(\mathbf{k})\,\mathrm{d}^3\mathbf{k},$$

$$d_{ij} = D_{ij}/q^2, \quad \tilde{d}_{ij} = d_{ij} - \frac{1}{3}\delta_{ij}. \tag{4}$$

Structure *circulicity* tensor:

$$F_{ij} = \int \mathscr{F}_{ij}(\mathbf{k})\,\mathrm{d}^3\mathbf{k},$$

$$f_{ij} = F_{ij}/q^2, \quad \tilde{f}_{ij} = f_{ij} - \frac{1}{3}\delta_{ij}. \tag{5}$$

Here $\mathscr{F}_{ij}(\mathbf{k})$ is the circulicity spectrum tensor, which is related to the vorticity spectrum tensor $W_{ij}(\mathbf{k}) = \overline{\hat{\omega}_i\hat{\omega}_j^*}$ through the relation

$$\mathscr{F}_{ij}(\mathbf{k}) = \frac{W_{ij}(\mathbf{k})}{k^2}.$$

We define the third-rank tensor

$$Q_{ijk} = -\overline{u_j'\Psi_{i,k}'}, \quad q_{ijk} = Q_{ijk}/q^2, \tag{6}$$

where we have used $q^2 = 2k = R_{ii}$ for the normalization. For homogeneous turbulence, Q_{ijk} is

$$Q_{ijk} = \epsilon_{ipq} M_{jqpk}, \tag{7}$$

where

$$M_{ijpq} = \int \frac{k_p k_q}{k^2} E_{ij}(\mathbf{k})\,\mathrm{d}^3\mathbf{k}. \tag{8}$$

The definition of the third-rank fully symmetric *stropholysis* tensor is given by

$$Q_{ijk}^* = \frac{1}{6}(Q_{ijk} + Q_{jki} + Q_{kij} + Q_{ikj} + Q_{jik} + Q_{kji}). \tag{9}$$

For homogeneous turbulence, Q_{ijk} and Q_{ijk}^* are bi-trace free

$$Q_{iik} = Q_{iki} = Q_{kii} = 0, \quad Q_{iik}^* = 0. \tag{10}$$

A decomposition based on group theory shows that Q_{ijk} and Q_{ijk}^* (here we use $q_{ijk}^* = Q_{ijk}^*/q^2$) are related to each other and to lower-rank tensors,

$$Q_{ijk} = q^2\left[\frac{1}{6}\epsilon_{ijk} + \frac{1}{3}(\epsilon_{ikm}r_{mj} + \epsilon_{jim}d_{mk} + \epsilon_{kjm}f_{mi}) + q_{ijk}^*\right], \tag{11}$$

and

$$r_{ij} = \epsilon_{imp}q_{mjp}, \quad d_{ij} = \epsilon_{imp}q_{pmj}, \quad f_{ij} = \epsilon_{imp}q_{jpm}. \tag{12}$$

3. Model formulation for homogeneous turbulence

The one-point structure-based model carries the transport equation for **Q** and a model transport equation for the dissipation rate ε. The formulation of the model is based on simplified non-local theory making use of structure modeling ideas. In Section 3.1, we outline this non-local theory and in Section 3.2, we show how it leads to the one-point model.

3.1. IPRM formulation

Kassinos and Reynolds (1994, 1996) formulated a simplified non-local theory particle representation model (PRM) for the rapid distortion theory (RDT) of homogeneous turbulence. The original idea was to represent the turbulence by an ensemble of fictitious particles. A number of key properties and their evolution equations are assigned to each particle. Ensemble averaging produces a representation of the one-point statistics of the turbulent field, which is exact for the case of RDT of homogeneous turbulence. In essence, this approach represents the simplest theory beyond one-point methods that provides closure for the RDT equations without modeling.

The interacting particle representation model (IPRM) is an extension of the PRM formulation that includes the effects of non-linear eddy–eddy interactions, important when the mean deformations are slow. Unlike standard models, which use return-to-isotropy terms, the IPRM incorporates non-linear effects through the use of effective gradients. The effective gradients idea postulates that the background non-linear eddy–eddy interactions provide a gradient acting on each particle in addition to the actual mean velocity gradient. An advantage of this formulation is the preservation of the RDT structure of the governing equations even for slow deformations of homogeneous turbulence. A detailed account of these ideas is given in Kassinos and Reynolds (1996, 1997) and will not be repeated here. To a large extent, the one-point Q-model is based on the IPRM formulation.

Each of the hypothetical particles in the IPRM is assigned a set of properties:

- **V** velocity vector,
- **W** vorticity vector,
- **S** stream-function vector,
- **N** gradient vector,
- P pressure.

The stream-function, velocity, and gradient vectors of each particle form an orthogonal triad, i.e.,

$$v_i = \epsilon_{irz}s_z n_r, \quad v_i v_j + s_i s_j + n_i n_j = \delta_{ij}, \tag{13}$$

where

$$n_i = N_i/N, \quad v_i = V_i/V, \quad s_i = S_i/S \tag{14}$$

are unit vectors.

In the IPRM, we follow the evolution of "clusters" of particles, each cluster representing a collection of particles having the same unit gradient vector n_i. Averaging over the particles of a given cluster produces conditional moments. Averaging the conditional statistics over all clusters produces the one-point statistics for the turbulent field. For homogeneous turbulence it is computationally efficient to track clusters rather than individual particles (Kassinos and Reynolds, 1996).

The governing equations for the conditional (cluster averaged) IPRM formulation are (see Kassinos and Reynolds, 1996)

$$\dot{n}_i = -G^n_{ki} n_k + G^n_{kr} n_k n_r n_i, \tag{15}$$

$$\dot{R}^{|\mathbf{n}}_{ij} = -G^v_{ik} R^{|\mathbf{n}}_{kj} - G^v_{jk} R^{|\mathbf{n}}_{ki} + [G^n_{km} + G^v_{km}](R^{|\mathbf{n}}_{im} n_k n_j + R^{|\mathbf{n}}_{jm} n_k n_i) - [2C_1 R^{|\mathbf{n}}_{ij} - C_2^2 R^{|\mathbf{n}}_{kk}(\delta_{ij} - n_i n_j)]. \tag{16}$$

Here $n_i(t)$ is the unit gradient vector and $R^{|\mathbf{n}}_{ij}$ is the conditional Reynolds stress tensor corresponding to a cluster of particles with a common $n_i(t)$. The effective gradients are

$$G^n_{ij} = G_{ij} + C^n G^e_{ij}, \quad G^v_{ij} = G_{ij} + C^v G^e_{ij}, \tag{17}$$

where G_{ij} is the mean velocity gradient and

$$G^e_{ij} = \frac{1}{\tau^*} r_{ik} d_{kj}.$$

The constants C^v and C^n are taken to be $C^n = 2.2$ $C^v = 2.2$. The different values for these two constants account for the different rates of return to isotropy of D_{ij} and R_{ij}.

The IPRM time scale τ^* is chosen so as to produce the proper dissipation rate for the turbulent kinetic energy. The rate of dissipation produced by the IPRM equation (16) is

$$\varepsilon^{\mathrm{PRM}} = q^2 \frac{C^v}{\tau^*} r_{ik} d_{km} r_{mi}. \tag{18}$$

We choose the time scale τ^* so that $\varepsilon^{\mathrm{PRM}} = \varepsilon$, where ε is the dissipation rate obtained from a model dissipation transport equation. This requires

$$\tau^* = \tau C^v r_{ik} d_{km} r_{mi}, \tag{19}$$

where τ is the turbulent time scale, which for homogeneous turbulence (at high Reynolds numbers) is simply q^2/ε. Thus to complete the IPRM, we use the standard model equation for the dissipation rate ε with a modification to account for the suppression of ε due to mean rotation,

$$\dot{\varepsilon} = -C_0 \frac{1}{\tau} - C_s S_{pq} R_{pq} \frac{1}{\tau} - C_\Omega \sqrt{\Omega_n \Omega_m d_{nm}}\,\varepsilon. \tag{20}$$

Here Ω_i is the mean vorticity vector, and the constants are

$$C_0 = \frac{11}{3}, \quad C_s = 3.0 \quad \text{and} \quad C_\Omega = 0.01. \tag{21}$$

The last term in (16) accounts for rotational randomization due to eddy–eddy interactions. We require that the rotational randomization model leaves the conditional energy unmodified. This requires that $C_1 = C_2^2$, and hence using dimensional considerations we take

$$C_1 = C_2^2 = 8.5\Omega^* f_{pq} n_p n_q, \tag{22}$$

where $\Omega^* = \sqrt{\Omega^*_k \Omega^*_k}$ and $\Omega^*_i = \epsilon_{ipq} G^e_{qp}$.

3.2. The stropholysis equation

We consider general deformations of homogeneous turbulence. The most convenient method for deriving the **Q** equation is to use the conditional (cluster averaged) IPRM formulation to obtain the evolution equation for **M** [see (8)], and then contract the **M** equation with the alternating tensor ϵ_{ijk} according to (7) in order to extract the **Q** equation. The PRM representation for **Q** and **M** is

$$Q_{ijk} = -\langle V^2 v_j s_i n_k \rangle, \quad M_{ijpq} = \langle V^2 v_i v_j n_p n_q \rangle, \tag{23}$$

where $s_i = \epsilon_{ikz} V_k n_z / V$ is the unit stream function vector (see Kassinos and Reynolds, 1997). Hence using (15) and (16) and the definitions (7) and (23), one obtains

$$\frac{\mathrm{d}Q_{ijk}}{\mathrm{d}t} = -G^v_{jm} Q_{imk} - G^n_{mk} Q_{ijm} - G^v_{sm} \epsilon_{its} M_{jmtk} - G^n_{mt} \epsilon_{its} M_{jsmk} + [G^n_{wq} + G^v_{wq}] Q_{iqwjk} + 2G^n_{qr} Q_{ijkqr} - 8.5\Omega^* f_{rs}[Q_{ijkrs} + Q_{jikrs}]. \tag{24}$$

Using the PRM representation, $Q_{ijkqr} = \langle V^2 v_j s_i n_k n_q n_r \rangle$.

3.3. Closure of the stropholysis equation

Closure of (24) requires a model for the tensor Q_{ijkpq} in terms of Q_{ijk}. Once such a model has been specified, it effectively provides a model for M_{ijpq} in terms of Q_{ijk} since M_{ijpq} can be obtained from Q_{ijkpq} by a contraction with ϵ_{ijk}. For small anisotropies, one can write an exact representation of Q_{ijkpq} in terms of Q_{ijk} that is linear in Q_{ijk}. Other tensors, like R_{ij}, D_{ij} and F_{ij}, can be expressed in terms of Q_{ijk} [see (12)] and need not be included explicitly in the model. Definitions (contractions and continuity) determine all the coefficients in the linear model. Thus the linear model contains no adjustable parameters.

In the presence of mean rotation, *rotational randomization* is an important dynamical effect that must be accounted for in the model. Rotational randomization, a strictly non-local effect that is lost in the averaging procedure generating the one-point statistics, is caused by the differential action of mean rotation on particle velocity vectors (Fourier modes) according to the alignment of the corresponding gradient (wavenumber) vectors with the axis of mean rotation. The main impact of Fourier randomization on one-point statistics is the damping of rotation-induced adjustments; here this effect is added explicitly through the simple model,

$$\frac{DQ_{ijk}}{Dt} = \cdots - \gamma_1(Q_{ijk} - Q^{rf}_{ijk}) - \gamma_2 \epsilon_{ijm}(R_{mk} - D_{mk}) - \gamma_3 \epsilon_{ikm}(F_{mj} - D_{mj}). \tag{25}$$

The first term accounts for the rotational randomization effects in rotation dominated flows, while the remaining two terms account for the modification of these effects due to the combined action of mean strain and rotation. $\mathbf{Q}^{rf}$ is the limiting state of **Q** under rapid rotation. Here γ_1, γ_2 and γ_3 are scalar functions of the invariants of the mean strain and rotation and are determined from simple test cases. A detailed discussion of these models will appear separately.

The new one-point model produces excellent results for general irrotational deformations of homogeneous turbulence. A particularly interesting example is shown in Fig. 1, where we consider the case of irrotational axisymmetric expansion (axisymmetric impingement). The mean velocity gradient tensor in this case is

$$S_{ij} = S \begin{pmatrix} -1 & 0 & 0 \\ 0 & \frac{1}{2} & 0 \\ 0 & 0 & \frac{1}{2} \end{pmatrix} \tag{26}$$

and the total strain

$$C = \exp\left(\int_0^t |S| t' \, \mathrm{d}t' \right) \tag{27}$$

is used as the horizontal axis in Fig. 1. As was discussed in Kassinos and Reynolds (1996, 1997), the axisymmetric expansion flow exhibits a paradoxical behavior, where a slower mean deformation rate produces a stress anisotropy that exceeds the one produced under RDT for the same total mean strain. This effect is triggered by the different rates of return to isotropy in the $\tilde{\mathbf{r}}$ and $\tilde{\mathbf{d}}$ equations, but it is dynamically controlled by the rapid terms. The net effect is a growth of $\tilde{\mathbf{r}}$ at the expense of $\tilde{\mathbf{d}}$, which is strongly suppressed. The one-point

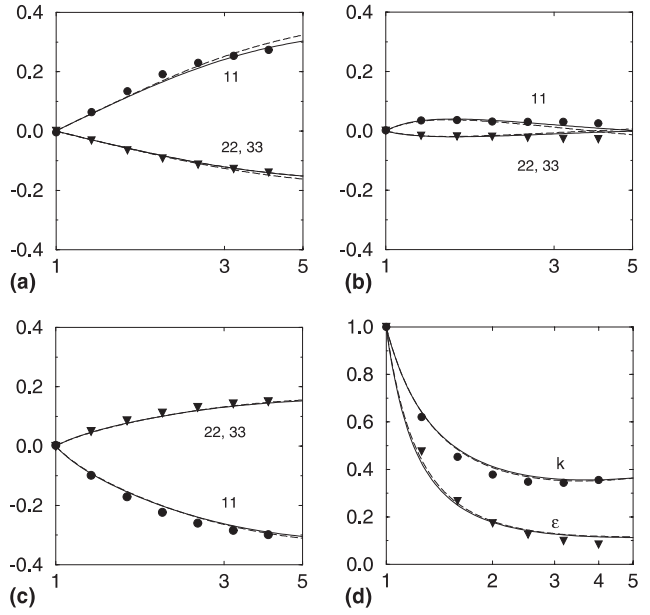

Fig. 1. Comparison of the one-point Q-model predictions (dashed lines) with IPRM results (solid lines) and the 1985 DNS by Lee and Reynolds (symbols) for the axisymmetric expansion case EXO ($Sq_0^2/\varepsilon_0 = 0.82$). (a)–(c) Evolution of the Reynolds stress, dimensionality, and circulicity anisotropies; 11 component (●), 22 and 33 components (▼). (d) Evolution of the normalized turbulent kinetic energy (●) and dissipation rate (▼).

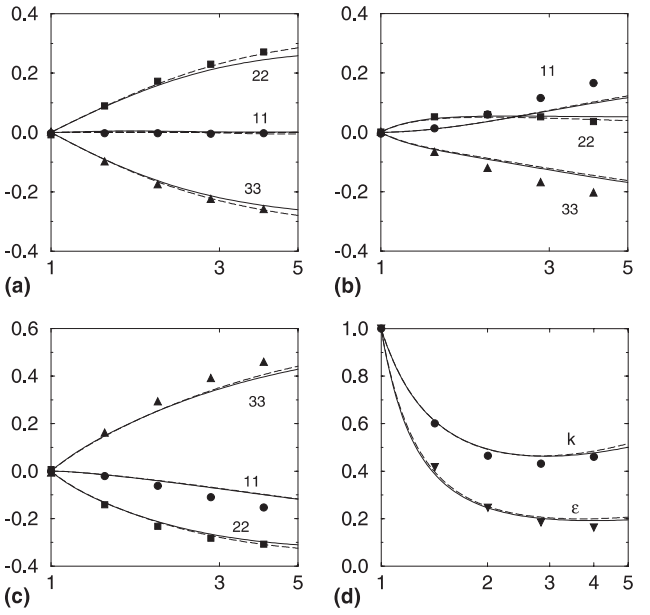

Fig. 2. Comparison of the one-point Q-model predictions (dashed lines) with the IPRM results (solid lines) and the 1985 DNS by Lee and Reynolds (symbols) for the plane strain case PXA ($Sq_0^2/\varepsilon_0 = 1.0$). (a)–(c) Evolution of the Reynolds stress, dimensionality, and circulicity anisotropies; 11 component (●), 22 component (■), 33 component (▲). (d) Evolution of the normalized turbulent kinetic energy (●) and dissipation rate (▼).

model (see Fig. 1) is able to capture these effects well and also predicts the correct decay rates for the normalized turbulent kinetic energy k/k_0 and dissipation rate $\varepsilon/\varepsilon_0$. The predictions of the one-point Q-model are comparable to those of the IPRM.

In Fig. 2, we consider deformation by plane strain

$$S_{ij} = S\begin{pmatrix} 0 & 0 & 0 \\ 0 & -1 & 0 \\ 0 & 0 & +1 \end{pmatrix}. \tag{28}$$

As shown in Fig. 2 (corresponding to $Sq_0^2/\varepsilon_0 = 1.0$) the performance of the one-point model is similar to that of the IPRM and its predictions compare favorably with the DNS results by Lee and Reynolds (1985). The details in the evolution histories of $\tilde{r}_{ij}, \tilde{d}_{ij}$ and $\tilde{f}_{ij}$ are captured well and the correct rates are predicted for the decay of the (normalized) turbulent kinetic energy k/k_0 and dissipation rate $\varepsilon/\varepsilon_0$.

The predictions of the one-point Q-model for the case of homogeneous shear (where the mean gradient is $G_{12} = \Gamma$) are shown in Fig. 3. Comparison is made to the DNS results by Rogers and Moin (1987). Note that the model produces satisfactory predictions for the components of $r_{ij} = R_{ij}/q^2, d_{ij} = D_{ij}/q^2$, and $f_{ij} = F_{ij}/q^2$. A fully developed state was reached in the simulations for $\Gamma t \geqslant 10$, and in this range both the Q-model and the IPRM predict the correct level for the dimensionless ratio of production over dissipation, P/ε. Here we define $P = -S_{ij}R_{ij}$.

A challenge for one-point models is found in the elliptic streamlines flow (see Fig. 4),

$$G_{ij} = \begin{pmatrix} 0 & 0 & -\gamma - e \\ 0 & 0 & 0 \\ \gamma - e & 0 & 0 \end{pmatrix}, \quad 0 < |\, e \,| < |\, \gamma \,|, \tag{29}$$

where the effects of mean rotation and plane strain are combined so as to emulate conditions encountered in turbomachinery. (Note that the case $e = 0$ corresponds to pure rotation

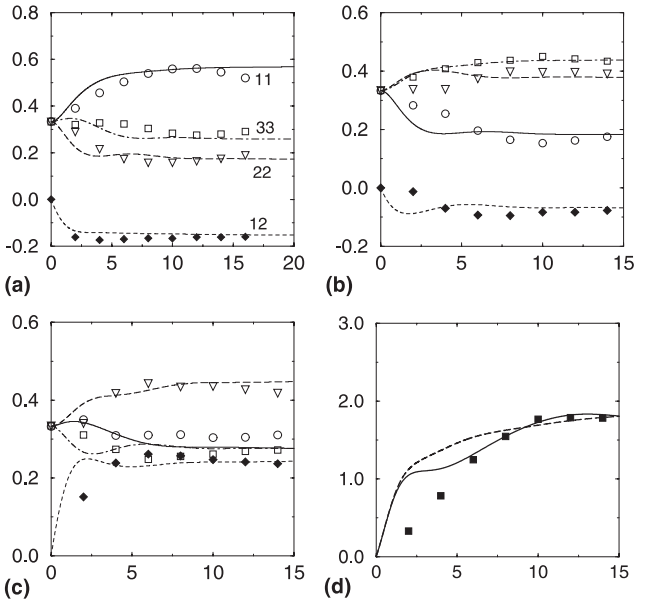

Fig. 3. Comparison of Q-model predictions (lines) and the 1987 DNS by Rogers and Moin (symbols). (a)–(c) Evolution of the Reynolds stress, dimensionality, and circulicity components in homogeneous shear with $\Gamma q_0^2/\varepsilon_0 = 4.72$: 11 component (———, ○); 22 component (– – – –, ▽); 33 component (– · –, □); 12 component (– – – –, ◆). (d) Evolution of production over dissipation rate (P/ε): model (– – – –); IPRM (———); DNS (■).

while the case $|\, e \,| = |\, \gamma \,|$ corresponds to homogeneous shear.) Direct numerical simulations (Blaisdell and Shariff, 1996) show exponential growth of the turbulent kinetic energy in elliptic streamline flows, the analysis of which shows they are

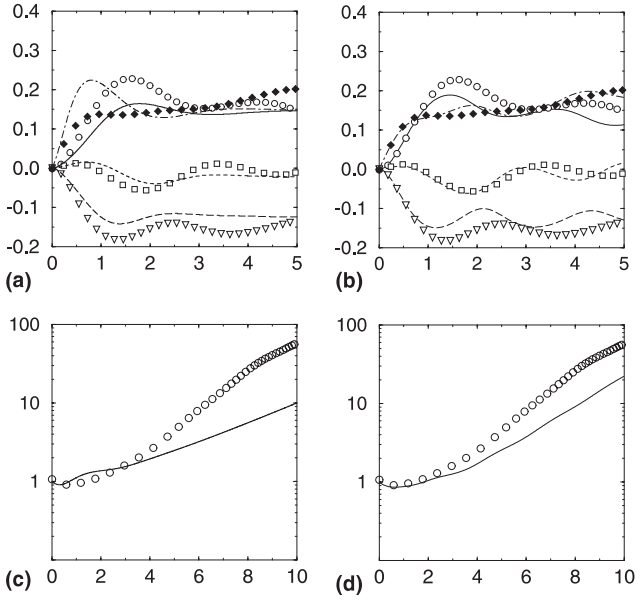

Fig. 4. Comparison of model predictions (lines) for the evolution of the Reynolds anisotropy in elliptic streamline flow ($E = 2.0$) with the 1996 DNS by Blaisdell and Shariff (symbols). (a) One-point Q-model vs DNS, (b) IPRM vs DNS: 11 component (———, ○); 22 component (– – – –, ∇); 33 component (– – – –, □); 13 component (–·–, ◆). Growth of the normalized turbulent kinetic energy: (c) one-point Q-model (line) vs DNS (symbols), (d) IPRM (line) vs DNS (symbols).

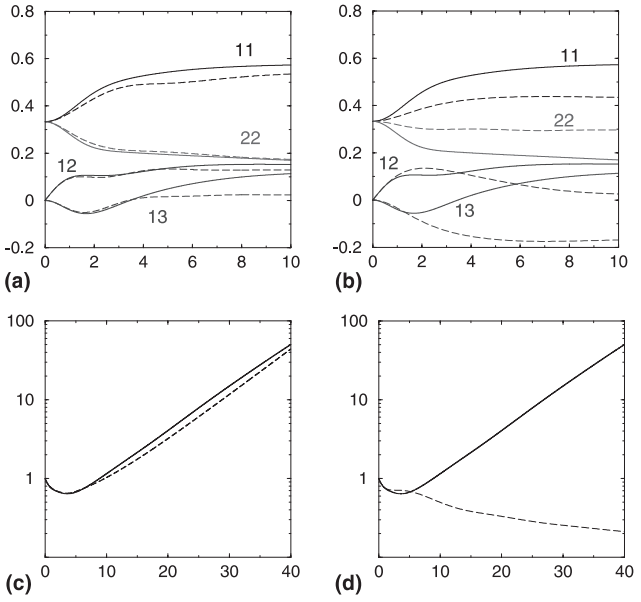

Fig. 5. Comparison of one-point model predictions (dashed lines) with those of two-point IPRM simulations (solid lines) for the homogeneous shear in a frame rotating about the streamwise direction ($\Gamma q_0^2/\varepsilon_0 = 4.72, \Omega^f/\Gamma = 1.0$). (a) One-point Q-model vs IPRM for the evolution of r_{ij}, (b) standard RST model vs IPRM for the evolution of r_{ij}, (c) one-point Q-model vs IPRM for the evolution of k/k_0, (d) standard RST model vs IPRM for the evolution of k/k_0.

associated with resonant instabilities in narrow wavenumber bands in wavenumber space. Standard RST models erroneously predict decay of the turbulence. As shown in Fig. 4, the one-point Q-model is able to capture the main features of the oscillations observed in the components of the Reynolds stress anisotropy $\tilde{r}_{ij}$. Furthermore, the model is able to capture an exponential growth of the turbulent kinetic energy. Note, however, that the initial growth rate predicted by both the non-local IPRM and the Q-model falls short of the rate predicted by the DNS. At longer times, the growth rates predicted by both models compare more favorably to those observed in the DNS.

A particularly interesting test case is that of homogeneous shear ($G_{12} = \Gamma$) in a frame rotating about the streamwise direction x_1

$$G_{ij} = \begin{pmatrix} 0 & \Gamma & 0 \\ 0 & 0 & 0 \\ 0 & 0 & 0 \end{pmatrix}, \quad \Omega_i^f = \Omega^f \delta_{i1}. \tag{30}$$

The configuration of this flow is similar to what one finds in turbulent flow through a rotating pipe, without of course the complications due to the presence of the pipe walls. Admittedly, some of those complications are vital in predicting rotating pipe flow, but nevertheless the simplified case considered here highlights the role played by the rapid pressure-strain-rate term in this family of flows, and brings to focus some of the limitations of standard RST models. This flow is a challenging test case for turbulence models because the streamwise rotation of the frame activates all three shear stresses and also components of the rapid-pressure strain rate term that are zero in homogeneous shear flow in a fixed frame. Some of the limitations of standard RST models are shown in Fig. 5, where we compare the predictions of the one-point Q-model and a standard RST model with those of a two-point (IPRM) simulation (DNS of this flow are currently being completed at Stanford University). As shown in Fig. 5(a) and (c), the Q-model predicts the correct sign for the stress component r_{13}. This is important because r_{13} affects the evolution of the shear stress r_{12}. The Q-model captures a reasonable level for r_{12} and therefore predicts an exponential growth of the turbulent kinetic energy in agreement with the two-point simulation. Standard RST models, however, an example of which is shown in Fig. 5(b) and (d), predict the wrong sign for r_{13}, and as a result they predict a vanishing shear stress r_{12} and as expected, a decreasing turbulent kinetic energy.

4. Inhomogeneous turbulence

The Q_{ijk} evolution equation for homogeneous turbulence [see (24) and (25)] is generalized in order to account for inhomogeneous effects (spatial gradients and wall blocking). Inhomogeneous effects are incorporated in the Q_{ijk} and ε equations through the addition of standard gradient diffusion models, accounting for turbulent transport, as outlined below

$$\frac{DQ_{ijk}}{Dt} = \mathcal{Q}_{ijk} + \frac{\partial}{\partial x_r}\left(\left[\nu\delta_{rs} + \frac{C_\nu}{\sigma_Q} R_{rs}\tau\right]\frac{\partial Q_{ijk}}{\partial x_s}\right), \tag{31}$$

$$\frac{D\varepsilon}{Dt} = \mathcal{E} + \frac{\partial}{\partial x_r}\left(\left[\nu\delta_{rs} + \frac{C_\nu}{\sigma_\varepsilon} R_{rs}\tau\right]\frac{\partial \varepsilon}{\partial x_s}\right), \tag{32}$$

where $\mathcal{Q}_{ijk}$ represents the right-hand side of Eq. (25), and $\mathcal{E}$ represents the right-hand side of Eq. (20). The turbulent kinetic energy is obtained from $k = \epsilon_{ikj}Q_{ijk}/2$. Following Durbin (1993), the coefficient of the production term in the ε equation is sensitized to the ratio of Production to dissipation as $C_s = 2.7(1 + 0.1P/\varepsilon)$.

Near-wall effects are incorporated in the Q-model through an elliptic relaxation scheme based on the ideas of Durbin.

In essence, terms in the transport Eq. (25) for Q_{ijk} that are not associated with either production or dissipation of the turbulent kinetic energy are lumped in a term named $\wp_{ijk}$. Thus, $\wp_{ijk}$ is a model for redistributive processes that is valid for homogeneous turbulence. We use kf_{ijk} to denote an augmented version of this model that is valid in inhomogeneous turbulence. kf_{ijk} reproduces satisfactorily near-wall redistributive processes, while reducing to $\wp_{ijk}$ sufficiently far from solid boundaries. The final form of the transport equation for Q_{ijk} is

$$\frac{DQ_{ijk}}{Dt} = -G_{jm}Q_{imk} - \frac{1}{2}G_{tm}\epsilon_{tik}R_{mj} + \frac{1}{2}G_{jm}(Q_{imk} + Q_{kmi}) - \frac{\varepsilon}{k}Q_{ijk} + kf_{ijk} + \frac{\partial}{\partial x_r}\left(\left[\nu\delta_{rs} + \frac{C_\nu}{\sigma_Q}R_{rs}\tau\right]\frac{\partial Q_{ijk}}{\partial x_s}\right), \quad (33)$$

where f_{ijk} is obtained by an elliptic relaxation equation,

$$L^2\nabla^2 f_{ijk} - f_{ijk} = -\wp_{ijk}/k, \quad (34)$$

and the simplest description of $\wp_{ijk}$ is

$$\wp_{ijk} = \mathcal{Q}_{ijk} + G_{jm}Q_{imk} + \frac{1}{2}G_{tm}\epsilon_{tik}R_{mj} - \frac{1}{2}G_{jm}(Q_{imk} + Q_{kmi}) + \frac{1}{\tau}Q_{ijk}. \quad (35)$$

The elliptic relaxation approach introduces some degree of non-locality back into the equations, which is particularly important near walls. The scheme described above allows us to capture the correct near-wall asymptotics and therefore the correct production of turbulent kinetic energy and the correct ratio of viscous to turbulent transport near the wall. Sufficiently far from the wall, $kf_{ijk} = \wp_{ijk}$, and the homogeneous model is recovered. This is in analogy to the elliptic relaxation scheme applied to RST models by Durbin.

At the wall k goes to zero, and so do the usual turbulent time and length scales. However, these scales should be finite at the wall, with a lower bound given by their Kolmogorov estimates. To reconcile these facts we define the time scale τ as a blending between the turbulent time scale k/ε and the Kolmogorov time scale, $(\nu/\varepsilon)^{1/2}$. Similarly the length scale L is a blending between the turbulent length scale $k^{3/2}/\varepsilon$ and the Kolmogorov length scale $(\nu^3/\varepsilon)^{1/4}$, along the lines of Pettersson et al. (1998).

4.1. Representative results

Preliminary results obtained with the Q-model for fully developed channel flow are encouraging. The model was implemented in a 1D-code using elliptic relaxation, as outlined above, and integrated throughout the entire domain, including the near-wall regions. A comparison of the Q-model predictions with DNS data (Moser et al., 1999) for fully developed channel flow at $Re_\tau = 395$ is shown in Fig. 6.

The Reynolds stress components (non-dimensionalized by the wall shear velocity u_τ) are shown in Fig. 6(a). The agreement between the model predictions (dashed lines) and the DNS (solid lines) is satisfactory. The model slightly overpredicts the peak in the streamwise component R_{11}^+ that occurs at about $y^+ \approx 15$. The components of the normalized Reynolds stress tensor $r_{ij} = R_{ij}/q^2$ are shown in Fig. 6(b). The agreement between the model predictions and the DNS results is again reasonable. The agreement in the case of the shear stress r_{12} is noteworthy. This is particularly important, since r_{12} is the only turbulent stress to provide coupling between the mean flow equation and the turbulence equations. The mean velocity profile is shown in Fig. 6(c). The model prediction is in good agreement with the DNS profile, the most notable difference being near the channel centerline. Finally, the model profile of the dissipation rate ε is shown in Fig. 6(d). The model is again in good agreement with the DNS, but has a larger wiggle near the wall than the data shown. This difference depends on the model transport equation for ε, and we are currently exploring

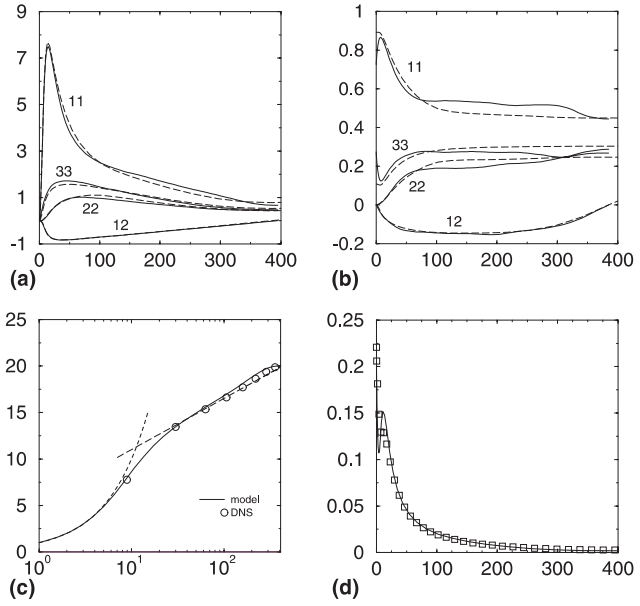

Fig. 6. Comparison of model predictions with DNS (Moser et al., 1999) for fully developed channel flow at $Re_\tau = 395$. (a) Components of the Reynolds stress tensor, (b) components of the Reynolds stress tensor normalized by its trace: model (– – ––); DNS (———). (c) mean velocity, (d) dissipation rate: model (———); DNS (□).

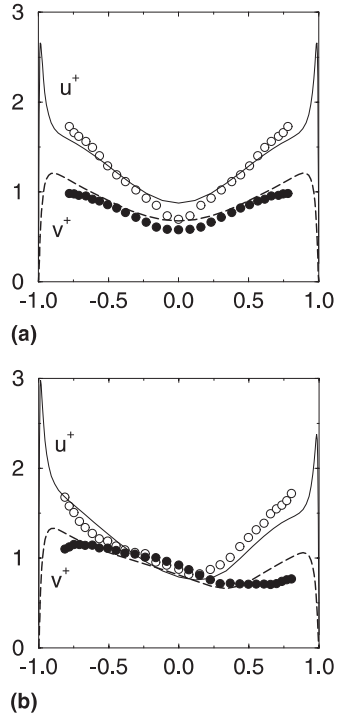

Fig. 7. Fully developed Poiseuille flow at $Re_\tau = 640$ with (a) no rotation and (b) with spanwise rotation ($Ro = 0.068$). Comparison of model predictions (lines) for the streamwise (u^+) and wall-normal (v^+) turbulence intensities with results from the LES (symbols) by Kim (1983).

alternative formulations that aim at taking full advantage of the structure information carried in the new model.

The Q-model has also been tested for fully-developed Poiseuille flow with system rotation. Here we consider rotation about the spanwise axis and compare results with the LES by Kim (1983) for the case $Re_\tau \equiv \overline{u}_\tau h/\nu = 640$ and $Ro \equiv 2h\Omega/U_b = 0.068$. The mean friction velocity $\overline{u}_\tau$ is computed using the wall shear stress averaged on the two walls, h represents the channel half-width, U_b is the bulk mean velocity across the channel, and Ω is the frame rotation rate.

A comparison of the model predictions for the turbulent intensities with the corresponding LES results is shown in Fig. 7. The fully developed case with no system rotation is also included [Fig. 7(a)] as a reference case. The agreement between the model predictions and the LES results for this reference case is acceptable. In the rotating case, the model is able to capture the characteristic asymmetry in the turbulent intensity profiles induced by the system rotation and overall agreement with the LES predictions is acceptable. The model correctly predicts that the wall normal intensity is significantly higher on the unstable (pressure) side than on the (stable) suction side of the channel. Near the channel centerline the model is able to capture the reversal of the stress anisotropy (v^+ becoming higher than u^+) due to frame rotation.

5. Conclusions

The turbulence structure affects the dynamics in non-equilibrium turbulence and its effects must be emulated by engineering models that are designed for use in complex flow regimes. This poses a challenge to traditional turbulence models which completely neglect turbulence structure. Here we outlined the construction of a new type of model that captures structure information missing from traditional one-point models. The model has been validated successfully for a wide range of deformations of homogeneous turbulence. Results obtained for simple wall-bounded flows are encouraging. We are currently evaluating the model in more complex flows.

Acknowledgements

This work has been supported by the Air Force Office of Scientific Research (under grants 95–0145 and 98–0138) and by the Center for Turbulence Research.

References

Blaisdell, G.A., Shariff, K., 1996. Simulation and modeling of the elliptic streamline flow. In: Proceedings of the 1996 Summer Program, Center for Turbulence Research, NASA-Ames/Stanford University.

Durbin, P.A., 1993. A Reynolds-stress model for near-wall turbulence. J. Fluid Mech. 249, 465–498.

Kassinos, S.C., Reynolds, W.C., Rogers, M.M., 1999. One-point turbulence structure tensors, J. Fluid Mech., submitted.

Kassinos, S.C., Reynolds, W.C., 1997. Advances in structure-based modeling, Annual Research Briefs 1997, Center for Turbulence Research, NASA-Ames/Stanford University.

Kassinos, S.C. Reynolds, W.C., 1996. An interacting particle representation model for the deformation of homogeneous turbulence, Annual Research Briefs 1996, Center for Turbulence Research, NASA-Ames/Stanford University.

Kassinos, S.C., Reynolds, W.C., 1994. A structure-based model for the rapid distortion of homogeneous turbulence, Report TF-61, Thermosciences Division, Department of Mechanical Engineering, Stanford University.

Kim, J., 1983. The effect of rotation on turbulence structure. In: Proceedings of the fourth Symposium on Turbulent Shear Flows, Karlsruhe, Germany, pp. 6.14–6.19.

Lee, M.J., Reynolds, W.C., 1985. Numerical experiments on the structure of homogeneous turbulence, Report TF-24, Thermosciences Division, Department of Mechanical Engineering, Stanford University.

Mahoney, J.F., 1985. Tensor and isotropic tensor identities. Matrix and Tensor Q 34 (5), 85–91.

Moser, R.D., Kim, J., Mansour, N.N., 1999. Direct numerical simulation of turbulent channel flow up to $Re_\tau = 590$. Phys. Fluids 11 (4), 943–945.

Pettersson, B.A., Andersson, H.I., Brunvoll, A.S., 1998. Modelling near-wall effects in axially rotating pipe flow by elliptic relaxation. AIAA J. 36 (7), 1164–1170.

Reynolds, W.C., Kassinos, S.C., 1995. A one-point model for the evolution of the Reynolds stress and structure tensors in rapidly deformed homogeneous turbulence. Proc. R. Soc. Lond. A, vol. 451, No. 1941, pp. 87–104.

Rogers, M.M., Moin, P., 1987. The structure of the vorticity field in homogeneous turbulent flows. J. Fluid Mech. 176, 33–66.